NUMERICAL STUDY ON COLD FORMED STEEL TUBULAR X-SECTION WITH DIFFERENT SUPPORT CONSTRAINTS

Mrs. K. Suganya Devi[1] & Mr Iyappan G. R[2]
B. R. Mohan, G. S. Kavitha, E. Santhosh, and M. N. Sivaranjan[3]
[1,2,3]Department of Civil Engineering, Valliammai Engineering College, Kattankulathur, Tamil Nadu, India

Abstract: This paper presents a comprehensive numerical investigation into the structural behaviour of cold-formed steel (CFS) circular hollow section (CHS) x-joints, with a specific focus on the quantitative influence of chord-end boundary conditions. While extensive research exists on the geometric and material parameters of such joints, the impact of support constraints which represents the joint's interaction with the larger structural system is often oversimplified. This study utilizes non-linear finite element analysis (FEA) to analyse a matrix of 90 models, examining the interplay between three brace-to-chord diameter ratios β, three brace intersection angles θ, and two reinforcement configurations (unreinforced and ring-stiffened). The central variable of the study is a spectrum of five distinct chord-end boundary conditions, ranging from fully fixed to fully free, including three nuanced variations of hinged supports with selective rotational freedoms. The results unequivocally demonstrate that the chord-end boundary condition is a dominant, first-order variable that can be more significant than geometric parameters. A key finding is the identification of a strong interaction effect: low β joints, which fail by chord-face "punching," are shown to be significantly more sensitive to boundary constraints than high-β joints, which engage the chord side-walls. Furthermore, the efficacy of external ring stiffeners is quantified, revealing a principle of diminishing returns, where stiffeners provide a substantial increase in capacity for flexible, free-end joints but offer only marginal benefit for joints that are already rigidly supported.

Keywords: - Cold-Formed Steel (CFS), Tubular X-Joints, Finite Element Analysis (FEA), Boundary Conditions, Ultimate Strength, Structural-System Interaction, Ring Stiffeners.

I. INTRODUCTION

A. Context: The Role of CFS in Modern Construction

In the pursuit of sustainable and efficient structural design, cold-formed steel (CFS) has emerged as a preferred material solution. Manufactured by roll-forming or press-braking steel at ambient temperatures, CFS sections are characterized by their thin-walled profiles, high geometric accuracy, and an exceptional strength-to-weight ratio. These properties translate directly into significant advantages in construction: reduced material usage, lower embodied carbon, decreased foundation loads, and expedited on-site assembly.

Within CFS frameworks, such as trusses and space frames, tubular hollow sections are frequently employed. The connections between these members are critical elements that govern the overall strength, stiffness, and integrity of the entire system. The X-joint, formed by the intersection of brace and chord members, is a fundamental connection type. Its primary function is to transfer axial loads from the braces to the chord member. However, this load transfer mechanism inherently creates high-stress concentrations at the brace-to-chord interface, making the X-joint a common point of failure. The structural behaviour of these joints is complex, often dictated by local phenomena such as chord face plasticization and local buckling rather than the gross strength of the members themselves.

B. Literature Review and Identification of Research Gaps

The structural performance of tubular joints has been the subject of extensive research. A significant portion of the literature has focused on the influence of material properties, particularly the use of high-strength steel (HSS) grades like S900 and S960, to enhance joint capacity. These studies have highlighted that existing design codes, such as Eurocode 3 and CIDECT provisions, are often overly conservative and uneconomical when applied to HSS, as they were developed based on the behaviour of conventional mild steel.

Other research avenues have explored the impact of geometric parameters, the behaviour of stainless-steel joints, and the development of advanced predictive models using finite element (FE) analysis and machine learning (ML) to overcome the high cost and time of physical testing.

Despite this broad body of work, a critical research gap persists: the systematic and nuanced investigation of chord-end boundary conditions. The vast majority of both numerical and experimental studies investigate joints under highly idealized support

conditions, typically "pinned" or "fixed". In reality, no joint in a structural frame exists in isolation. It is part of a larger system, and its chord member is continuous, connecting to flexible beams or semi-rigid columns. This "structural-system interaction" means that the true restraint condition of a chord is almost always semi-rigid, falling somewhere on the spectrum between the two theoretical extremes.

This oversimplification of boundary conditions is a significant omission. The assumption that supports conditions are a secondary or negligible effect is a hypothesis that has not been adequately tested. This paper posits that the chord-end boundary condition is, in fact, a primary-order variable that can fundamentally alter the joint's load-carrying mechanism, failure mode, and ultimate capacity.

C. Objectives and Scope

The primary objective of this paper is to numerically quantify the influence of a comprehensive spectrum of five distinct chord-end boundary conditions on the ultimate capacity of CFS tubular X-joints. These conditions range from fully fixed to fully free and include three discrete, rotationally-defined hinged cases to simulate semi-rigid behaviour.

Secondary objectives are:

1. To analyse the interaction between these boundary constraints and key geometric parameters, specifically the brace-to-chord diameter ratio β and the brace intersection angle θ.

2. To evaluate the variable efficacy of an external ring stiffener, quantifying how its performance is coupled to the inherent stiffness of the support condition.

To achieve these goals, a large-scale parametric study was conducted using the finite element method (FEM). The study comprises 90 distinct 3-D non-linear models, providing a robust dataset to analyse these complex interactions and propose more nuanced design considerations.

II. FINITE ELEMENT MODELING FRAMEWORK

The numerical investigation was executed entirely using the ANSYS Workbench 2023 finite element analysis software. The methodology was designed to systematically isolate the variables under investigation, ensuring that the results are comparable and reliable.

A. Model Geometry and Material Properties

The parametric study was built around a matrix of geometric, boundary, and reinforcement variables. All models used Circular Hollow Section (CHS) members for both the chord and brace. The brace diameter (76 mm), brace and chord lengths (600 mm), and member thickness (3 mm) were held constant across all models.

The primary variables for each model were:

- **Brace-to-Chord Ratio β:** Three ratios were investigated: 1.0, 0.75, and 0.5. These were achieved by varying the chord diameter (76 mm, 101 mm, and 152 mm, respectively).
- **Brace Intersection Angle θ:** Three angles were modelled: 90°, 45°, and 30°.
- **Reinforcement:** Each geometric configuration was modelled twice: once as an unreinforced joint and once with an external 3 mm thick ring stiffener.
- **Boundary Conditions:** Each of the above configurations was analysed under five distinct chord-end support conditions (detailed in Section II.C), resulting in a total of 90 models.

The material for all components was modelled as standard structural steel, commonly used for cold-formed sections. The mechanical properties adopted for the analysis are summarized in Table I.

Table I. Geometric Parameters and Material Properties

Brace diameter	B_d	76 mm
Chord diameter	C_d	76mm,101mm, 152mm
Brace angle	Θ	30° 45°, 90°
B ratio	B	0.5, 0.75, 1.0
Brace length	B_l	600mm
Chord length	C_l	600mm

B. Meshing Strategy and Analysis Type

To ensure accurate capture of high stress gradients and local buckling phenomena, a deliberate meshing strategy was employed. The models were discretized using 10-node tetrahedral solid elements (SOLID187 in ANSYS). This higher-order element is well-suited for modelling the curved geometries of tubular intersections and capturing complex stress states without exhibiting shear locking.

A non-uniform meshing strategy was implemented to balance computational cost with solution fidelity. A relatively coarse mesh was applied to regions of the chord and brace far from the intersection, where stress gradients were expected to be low. In contrast, a significant mesh refinement was applied to the critical area at and surrounding the brace-chord intersection,

as shown in Fig. 1. This local refinement ensures that peak stresses, plastic deformation, and the initiation of local buckling are captured with high precision, a practice consistent with established methodologies for tubular joint analysis. The analysis was conducted as a Static Structural analysis with the 'Large Deflection' setting activated to account for geometric non-linearities, which are essential for capturing buckling behaviour.

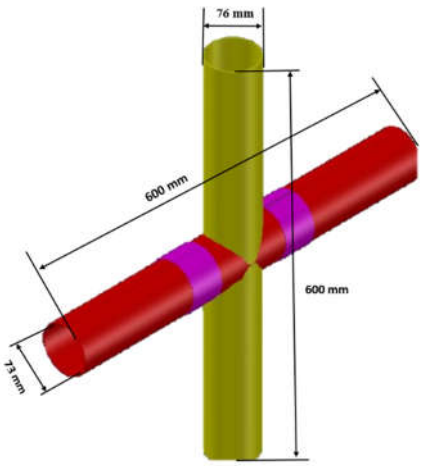

Fig. 1. Geometric configuration and key dimensions of the CHS X-joint model.

C. Implementation of Boundary Conditions and Loading

The definition of loads and boundary conditions is the most critical aspect of this study's methodology.

Loading: A compressive axial load was applied to the brace. To ensure stability and trace the post-peak response, a displacement-controlled load was simulated by applying a prescribed downward displacement to a rigid plate coupled to the top surface of the brace. The bottom end of the brace was fully fixed (all translational and rotational degrees of freedom constrained). The total reaction force at the point of displacement application was monitored to generate the load-displacement curve, from which the ultimate load capacity (P_u) was determined.

Chord-End Constraints: The five distinct support cases for the chord ends were implemented as follows:

1. **Fixed (Fixed):** Represents a fully rigid connection. All nodes on both end faces of the chord were fully constrained (all translational (UX, UY, UZ) and rotational (ROTX, ROTY, ROTZ) degrees of freedom (DOFs) set to 0).
2. **Free (Free):** Represents a complete lack of restraint. No constraints were applied to the chord end faces.
3. **Hinged 1 (H1: Free,0,0):** Simulates a pin connection allowing only torsion about the chord's longitudinal axis (assumed X-axis). Translational DOFs were fixed (UX, UY, UZ = 0). Rotational DOFs were set to (ROTX = Free, ROTY = 0, ROTZ = 0).
4. **Hinged 2 (H2: Free, Free,0):** Simulates a hinge allowing torsion and in-plane bending. Translational DOFs were fixed (UX, UY, UZ = 0). Rotational DOFs were set to (ROTX = Free, ROTY = Free, ROTZ = 0).
5. **Hinged 3 (H3: Free, Free, Free):** Simulates a perfect ball-joint, allowing unrestricted rotation in all directions. Translational DOFs were fixed (UX, UY, UZ = 0). Rotational DOFs were set to (ROTX = Free, ROTY = Free, ROTZ = Free).

The three hinged variations (H1, H2, H3) were implemented using the "Remote Displacement" feature in ANSYS. This is a key methodological innovation of this study. This feature works by coupling all the nodes on the circular end face of the chord to a single remote point located at the centre of that face. The translational and rotational constraints are then applied to this single remote point, allowing for a precise and computationally stable simulation of a true hinged connection with selective release of rotational DOFs.

D. Model Validation

Establishing the credibility of the finite element model is a prerequisite for a parametric study. As direct experimental validation for all 90 specific geometries was not feasible within the scope of this project, a widely accepted two-part validation strategy was adopted.

1. **Methodological Validation:** The modelling methodology encompassing the choice of SOLID187 elements, the non-uniform meshing strategy, the use of Large Deflection analysis, and the implementation of boundary conditions was systematically aligned with best-practice procedures from previously published research. These referenced studies have themselves been successfully validated against experimental data, providing a strong precedent for the soundness of the approach used here.
2. **Qualitative Validation:** The simulation outputs were critically examined for physical plausibility. The deformed shapes and stress contour plots obtained from the unreinforced models consistently showed the highest stress concentrations at the saddle and crown positions of the brace-chord intersection and the maximum deformation (dishing) on the chord face directly under the brace footprint. This behaviour is entirely consistent with the well-documented physical failure modes of tubular X-joints, providing a high degree of confidence that the model is capturing the

correct structural response and load-transfer mechanisms.

For a comparative parametric study of this nature, this validation approach is sufficient. It confirms that the model accurately captures the mechanisms of failure, which ensures that the relative differences in ultimate load observed between the models are a valid and reliable basis for drawing conclusions.

III. RESULTS: PARAMETRIC ANALYSIS OF UNREINFORCED JOINTS

This section presents the synthesized results for the 45 unreinforced joint models. In accordance with the objective of providing a clear, high-level analysis, the raw numerical data from the 45 simulations are not presented in tabular form. Instead, the ultimate load (P_u) data are synthesized and presented exclusively in the three following comparative graphs. Each graph corresponds to a brace intersection angle θ and plots the ultimate load capacity as a function of the five chord-end boundary conditions for all three β ratios.

A. Influence of Boundary Conditions at 90° Intersection (θ=90°)

Fig. 2 presents the results for the nine unreinforced models with a 90° brace intersection. This graph clearly illustrates the dominant influence of the chord-end boundary conditions.
Analysis of the 90° data reveals three critical findings:

1. **Clear Hierarchy:** A distinct hierarchy of strength is evident. The 'Fixed' condition, providing full rotational and translational restraint, consistently yields the highest ultimate capacity for all β ratios. Conversely, the 'Free' condition, offering no restraint, results in the lowest capacity.

2. **BC-Sensitivity and β Ratio Interaction:** The impact of the boundary condition is not uniform; it is strongly dependent on the β ratio. For the β=0.5 joint (where the brace "punches" the chord face), the capacity plummets by nearly 88% from the 'Fixed' (195.59 kN) to the 'Free' (23.72 kN) condition. In contrast, for the β=1.0 joint (where the load is transferred more to the chord side-walls), the drop is a more moderate 48% (from 465.88 kN to 242.6 kN). This identifies a crucial interaction: **low β (punching) joints are far more sensitive to the chord's end-restraint** than high β joints.

3. **Non-linear Hinge Behaviour:** The behaviour of the three hinged-support variations (H1, H2, H3) is not a simple linear progression from 'Fixed' to 'Free'. For the β=1.0 case, the 'H3' condition (all rotations free) is counter-intuitively stronger (421.69 kN) than both 'H1' (388.33 kN) and 'H2' (378.56 kN). This suggests that the partial rotational restraints of H1 and H2 may introduce adverse secondary bending or torsion, while the "perfect" ball-joint of H3 allows the chord to favourably realign and redistribute stresses more effectively.

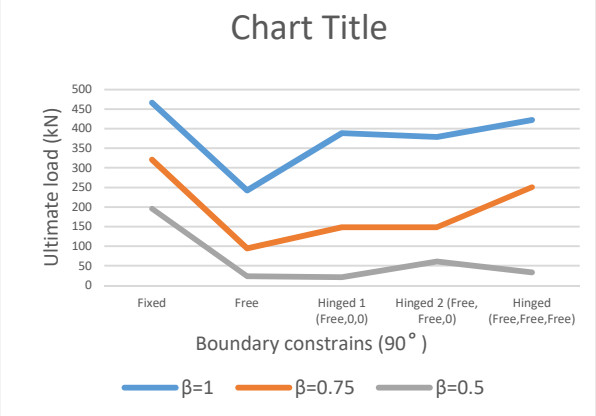

Fig. 2. Comparison of ultimate load (kN) for 90-degree X-joints across five chord-end boundary conditions, grouped by β-ratio.

B. Influence of Boundary Conditions at 45° Intersection (θ=45°)

Fig. 3 presents the results for the 45^0 intersections. This configuration introduces an elongated brace "footprint" on the chord, but the fundamental trends observed at 90^0 are largely confirmed.

The 'Fixed' condition remains superior across all β ratios. The extreme sensitivity of the β =0.5 joint is reiterated, with its capacity dropping by 74% from 'Fixed' (90.64 kN) to 'Free' (24.40 kN). The complex, non-linear behaviour of the hinged supports is also present, although the relative ranking of H1, H2, and H3 shifts, indicating a complex interplay between the intersection angle, β ratio, and the specific rotational DOFs being restrained.

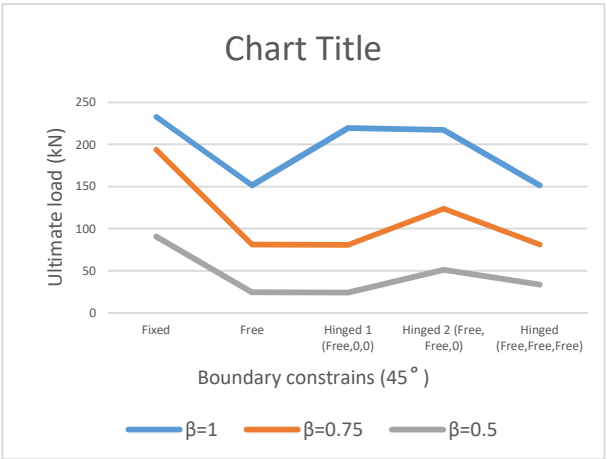

Fig. 7. Comparison of ultimate load (kN) for 45-degree X-joints across five chord-end boundary conditions, grouped by β ratio.

C. Influence of Boundary Conditions at 30° Intersection (θ=30°)

Fig. 4 completes the unreinforced analysis by presenting the data for the most acute intersection angle, 30^0. At this angle, the brace's axial force has a smaller perpendicular component acting on the chord face, and the intersection footprint is at its longest.

The results from the 30^0 models are consistent with the previous findings. The 'Fixed' and 'Free' conditions continue to act as the upper and lower bounds of structural capacity. The sensitivity of the lower β ratio joints remains the most significant finding; the capacity of the β =0.75 joint, for example, is over 5.5 times higher in the 'Fixed' condition (177.86 kN) than in the 'Free' condition (32.33 kN).

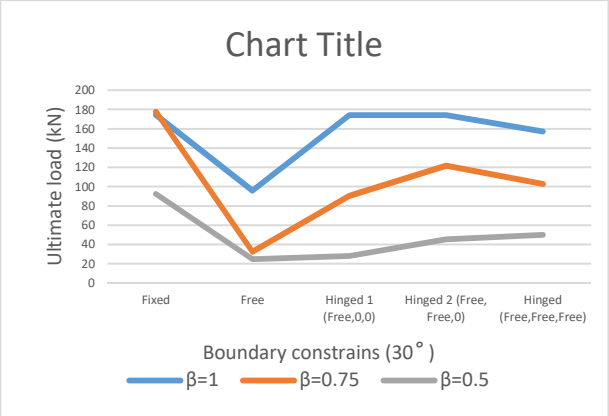

*Fig 4. Comparison of ultimate load (kN) for **30-degree** X-joints across five chord-end boundary conditions, grouped by β-ratio.*

D. Visualization of Failure Modes

The quantitative data presented in Figs. 2-4 can be explained by examining the qualitative failure modes. The FEA results provide clear visualizations of deformation and stress, as shown in Fig. 6.

The simulation outputs confirm the two primary mechanical behaviours:

- **Low β Failure:** For low β ratios (e.g., 0.5), the brace footprint is small relative to the chord diameter. The failure is dominated by **chord face plasticization** (also known as "dishing" or "punching shear"). The chord face acts like a flexible membrane, and its capacity is highly dependent on its ability to resist this local indentation.
- **High β Failure:** For high β ratios (e.g., 1.0), the brace intersects near the chord's sides. The load is no longer just "punched" through the face; it is transferred to the **chord side-walls**, which engage in resisting the load. The failure mode becomes a combined one, involving both chord face indentation and buckling of the chord side-walls.

This visual evidence provides the mechanical explanation for the interaction effect identified in Section III.A. Because the low β joint relies entirely on the chord face for its strength, its capacity is extremely sensitive to end-restraints ('Fixed' vs. 'Free') which directly influence the stiffness of that face. The high β joint, by engaging the side-walls, has a more robust load path that is inherently less dependent on the end-restraints.

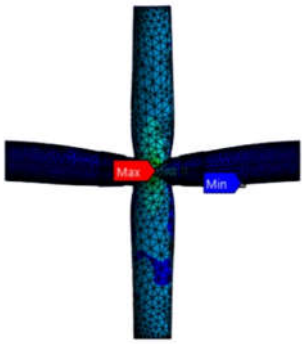

Fig 6. Deformation and stress distribution

IV. EFFICACY OF EXTERNAL RING STIFFENERS

The second phase of the investigation analysed the 45 models again, this time with a 3 mm external ring stiffener added to the joint. The primary purpose of a stiffener is to bolster the local stiffness of the chord wall, prevent premature local failure, and thereby increase the joint's ultimate capacity.

A. Strength Enhancement Factor (SEF) Analysis

To provide a direct, normalized measure of the stiffener's benefit, the **Strength Enhancement Factor (SEF)** was calculated for each of the 45 configurations. This metric is defined as the percentage increase in ultimate load capacity of the reinforced joint relative to its identical unreinforced counterpart:

$$\text{SEF (\%)} = \frac{(P_{u,reinforced} - P_{u,unreinforced})}{(P_{u,unreinforced})} \times 100\%$$

This SEF value allows for a clear comparison of the relative improvement provided by the stiffener, isolating its efficacy from all other geometric and boundary variables.

B. Interaction of Reinforcement and Support Stiffness

The most significant finding from the reinforced-joint analysis is the powerful interaction between the stiffener's effectiveness (SEF) and the chord's boundary condition. The results, summarized from the data in the source report, show that the stiffener's benefit is not absolute; it is highly dependent on the pre-existing stiffness of the joint.
This is the **principle of diminishing returns**. The fixed-end boundary condition and the ring stiffener

serve the same functional purpose: they both add local stiffness to the chord face to prevent plasticization.

- In a **Fixed** system, the boundary condition has already provided a high degree of stiffness and strength to the joint. The ring stiffener, when added, is functionally redundant. It adds some benefit, but its contribution is marginal compared to the strength already provided by the supports.

- In a **Free** or flexible system, the chord face is the primary point of weakness. The ring stiffener acts as a critical local brace, directly counteracting this primary failure mode. Its contribution is therefore massive, leading to a very high relative gain in strength.

This principle is clearly visible in the data. For example, in the β=0.75, $45° configuration, the stiffener provides a remarkable **83.4%** strength boost (SEF) for the flexible 'Free' joint. However, for the identical joint under the rigid 'Fixed' condition, the same stiffener provides only a **35.6%** boost. The 'Fixed' joint was already strong, so the stiffener's relative impact was much lower.

This demonstrates that the decision to use reinforcement cannot be made in isolation. Its cost-effectiveness is inextricably linked to the support conditions of the member it is intended to strengthen. It is also noted that in a few isolated cases (e.g., β =0.5, 90°, Free-End), the analysis returned a negative SEF, meaning the stiffened joint was weaker. This is not an error, but rather an indication of a complex failure mode shift. By preventing the ductile chord-face failure, the stiffener forced a different, more brittle, and premature failure to occur at a lower load, (e.g., local buckling near the stiffener weld or a different instability mode), highlighting the complex trade-offs in joint design.

V. DISCUSSION AND DESIGN IMPLICATIONS

The numerical results of this 90-model study yield several high-level conclusions that have direct implications for structural design and the refinement of building codes.

A. The Fallacy of Pinned vs Fixed

The primary contribution of this paper is the demonstration that the simple "pinned" or "fixed" binary, commonly used in design models, is a gross oversimplification that can lead to inaccurate and potentially unsafe or uneconomical designs. The results from the three-stage hinge models (H1, H2, H3) prove that joint capacity is highly sensitive to which rotational DOFs are restrained. The non-linear and sometimes counter-intuitive results (e.g., H3 being stronger than H1) show that the relationship between rotational restraint and ultimate capacity is complex. This challenges the assumptions in existing design codes and highlights the need for a more sophisticated, spectrum-based approach to modelling support conditions.

B. Design Guideline 1: BC-Sensitivity is a Function of β Ratio

The clear interaction effect identified in Section III.A leads to a practical design guideline.

- **Implication:** For joints with **low β ratios** (β 0.5), the failure is by "punching," and the joint's capacity is critically dependent on the chord's end-restraint. An engineer must have a high-confidence assessment of the chord's boundary condition to accurately predict the joint's strength. Using a simple "pinned" assumption for a joint that is, in reality, semi-rigid could be dangerously unconservative.
- For joints with **high** β **ratios** (β 1.0), the load is transferred to the side-walls, and the capacity is less sensitive to the end-restraints. In these cases, a simplified assumption may be more justifiable.

C. Design Guideline 2: Stiffener Efficacy is a Function of BC-Stiffness

The "diminishing returns" principle from Section IV provides a powerful, cost-saving recommendation.

- **Implication:** Engineers should prioritize the use of ring stiffeners on joints where the chord member is flexible or has long, unrestrained spans (approaching a 'Free' condition). In these applications, the stiffener provides the maximum possible benefit (e.g., +83.4% capacity) and is highly cost-effective.
- Conversely, engineers can potentially omit stiffeners on joints where the chord member is rigidly supported (e.g., connecting directly to a stiff column, approaching a 'Fixed' condition). In this scenario, the stiffener is redundant and provides minimal relative benefit, making it an inefficient use of material and fabrication cost.

D. Future Work

This numerical study provides a comprehensive foundation, but further work is required. The most critical next step is the experimental validation of these findings, particularly the non-linear behaviour of the hinged supports and the "diminishing returns" principle for stiffeners. Future numerical studies could also apply this 5-BC analysis framework to other joint types (K, T, Y), as well as to joints fabricated from HSS or stainless steel.

VI. CONCLUSION

This paper presented a 90-model finite element investigation on the ultimate strength of CFS tubular X-joints, focusing on the dominant, and often overlooked, influence of chord-end boundary conditions. The analysis systematically examined the interplay between five distinct support constraints, three β -ratios, three intersection angles, and the presence of ring stiffeners.

The principal findings of this research are:

- **Dominant Variable:** Chord-end boundary conditions are a dominant, first-order variable that can control the ultimate load capacity. The difference between a 'Fixed' and 'Free' end condition can alter the joint strength by over 550% (a factor of 5.5) in some configurations.
- **Complex Hinge Behaviour:** The behaviour of semi-rigid (hinged) supports is complex and non-linear. The joint capacity is highly sensitive to the specific degrees of rotational freedom that are restrained, proving that the traditional "pinned" or "fixed" design assumptions are inadequate.
- **BC β Interaction:** A novel interaction effect was identified and explained: low-β (punching) joints are significantly more sensitive to chord-end boundary conditions than high-β (side-wall) joints.
- **Stiffener Efficacy Principle:** A "principle of diminishing returns" for reinforcement was quantified. The effectiveness of a ring stiffener is inversely proportional to the inherent stiffness of the boundary condition. Stiffeners provide the greatest relative benefit on the most flexible joints.

These findings provide a more nuanced understanding of tubular joint behaviour, emphasizing the critical importance of system-level interactions. The design guidelines derived from this analysis can help engineers make more accurate, economical, and safe decisions in the design of CFS structures.

REFERENCES

1. P. Thangavel et al., "This research investigates the finite element analysis (FEA) of cold-formed steel (CFS) L-columns with pin-ended supports under compression," 2025.
2. M. Pandey et al., "Conducted a detailed numerical and experimental investigation on the cold-formed high-strength steel (CFHSS) CHS-to-RHS X-joints made from S900 and S960 steel grades," 2023.
3. S. H. Kim et al., "Presented a numerical and machine learning (ML) approach to predict the strength of steel circular hollow section (CHS) X-joints with high accuracy," 2024.
4. G. Irsel et al., "Developed and analyzed a thin-walled hollow X-section beam designed for lightweight structural applications where weight reduction and strength efficiency are critical," 2023.
5. J. Havula, M. Garifullin, M. Heinisuo, K. Mela, and S. Pajunen, "Moment-rotation behaviour of welded tubular high strength steel T-joint," Engineering Structures, vol. 172, pp. 523-537, 2018.
    A. Haakana, "In-plane buckling and semi-rigid joints of tubular high strength steel trusses," M.Sc. Thesis, Tampere University of Technology, Tampere, 2014.
6. X. Lan and T. M. Chan, "Recent research advances of high strength steel welded hollow section joints," Structures, vol. 17, pp. 58-65, 2019.
7. M. Garifullin, K. Mela, and M. Heinisuo, "Experimental and numerical study on the static strength of welded S960 high-strength steel RHS K-joints," Thin-Walled Structures, vol. 155, p. 106917, 2020.
8. F. Simon, M. Moradi, J. Hildebrand, and H. Pasternak, "Mechanical behaviour of welded high strength steel rectangular hollow section K-joints," Journal of Constructional Steel Research, vol. 183, p. 106720, 2021.
9. T. M. Chan, B. Young, and W. Y. Lam, "Numerical investigation on the ultimate capacity of high-strength steel CHS X-joints under axial loading," Engineering Structures, vol. 241, p. 112461, 2021.
10. W. Chen, T. M. Chan, and B. Young, "Finite element analysis of cold-formed steel multi-limb members with high-strength steel and corner radius effects," Thin-Walled Structures, vol. 195, p. 111516, 2024.
11. H. Yang, J. Fan, Z. Yang, and L. H. Han, "Seismic performance of high-strength steel welded RHS T-joints," Journal of Constructional Steel Research, vol. 209, p. 108035, 2023.
12. X. Li, J. Li, K. Zhou, and C. Zhao, "Experimental and numerical study of circular high-strength steel T-joints under in-plane bending," Engineering Structures, vol. 298, p. 117071, 2024.
13. J. Liu, Y. Wang, and G. Li, "Advanced finite element modelling of bolted steel connections: A review," Archives of Computational Methods in Engineering, 2024.
14. J. Fang, C. Sun, and G. Q. Li, "A comprehensive FE model for progressive collapse analysis of steel structures," Journal of Constructional Steel Research, vol. 200, p. 107693, 2023.

15. D. Xia and L. Shi, "Finite element analysis of steel truss bridge structure based on ANSYS," Journal of Engineering Research and Reports, vol. 25(9), 2023.
16. X. Lan, T. M. Chan, and B. Young, "Fatigue behaviour of high-strength steel welded circular hollow section joints under constant and variable amplitude loading," International Journal of Fatigue, vol. 134, p. 105494, 2020.
    A. Saliba, M. D'Aniello, and T. Fasanella, "The effect of the plate width on the capacity of high-strength steel welded joints," Structures, vol. 54, pp. 52-64, 2023.
17. J. J. L. P. da Silva, M. E. Goulart, and L. M. C. Simões, "Numerical investigation on the structural performance of steel-concrete-steel sandwich wall panels using high-strength steel," Thin-Walled Structures, vol. 183, p. 110290, 2023.
18. H. Hafez, T. El-Sayed, and S. El-Khoriby, "Deep learning-based predictive model for the ultimate strength of cold-formed steel columns," Engineering Structures, vol. 290, p. 116347, 2023.
19. CEN, Eurocode 3: Design of Steel Structures – Part 1-8: Design of Joints (EN 1993-1-8:2024), Brussels, 2024.
20. CEN, Eurocode 3: Design of Steel Structures – Part 1-5: Plated Structural Elements (EN 1993-1-5:2024), Brussels, 2024.
21. CEN, Eurocode 3: Design of Steel Structures – Part 1-1: General Rules and Rules for Buildings (EN 1993-1-1:2022), Brussels, 2022.
22. K.-J. Bathe, Finite Element Procedures, 2nd ed. Watertown, MA, USA: Klaus-Jurgen Bathe, 2006.
23. American Institute of Steel Construction (AISC), AISC 360-23: Specification for Structural Steel Buildings, Chicago, IL, 2023.